J|A|C|S ARTICLES

Published on Web 05/04/2010

Analytical Model for Rates of Electron Attachment and Intramolecular Electron Transfer in Electron Transfer Dissociation Mass Spectrometry

Jack Simons

Chemistry Department and Henry Eyring Center for Theoretical Chemistry, University of Utah, Salt Lake City, Utah 84112

Received January 11, 2010; E-mail: simons@chem.utah.edu

Abstract: A new physical model is put forth to allow the prediction of electron transfer rates and distances for (i) intramolecular transfer from an $n \geq 3$ Rydberg orbital on a positive site to a disulfide or amide bond site and (ii) intermolecular transfer from an anion donor to an $n \geq 3$ Rydberg orbital of a positively charged polypeptide. Although ab initio methods have proven capable of handling such electron transfer events when the Rydberg orbital has principal quantum number $n = 3$, they have proven to be incapable of handling Rydberg states having quantum number $n > 3$, so having a new tool capable of handling $n > 3$ Rydberg states is important. The model (i) focuses on each Rydberg orbital's large peak of high amplitude, (ii) approximates the electron density within this peak as constant within a radial shell characterized by a radius $<r>$ and thickness T both of which depend on the quantum number n, and (iii) assumes that strong coupling (either with an orbital of an anion donor or to a disulfide σ^* or a backbone amide π^* orbital) occurs when the valence orbital penetrates fully within the radial shell of the Rydberg orbital. These assumptions permit a derivation of the ratios of rates of electron transfer for $n > 3$ to those for $n = 3$. Combining these ratios with ab initio rates for $n = 3$ allows one to make rate predictions for inter- and intramolecular electron transfer involving Rydberg orbitals appropriate to the electron transfer dissociation process. One important prediction of this model is that the *combination* of large-penetration and Landau−Zener surface-crossing conditions places very severe limitations on which Rydberg levels can initially be populated in electron transfer dissociation. Another prediction is that a Rydberg orbital of a given principal quantum number n has a limited range of distances over which it can transfer an electron; σ^* or π^* orbitals either too far from *or too close* to a given Rydberg orbital cannot accept an electron from that orbital.

1. Introduction

In electron-capture dissociation[1−4] (ECD) experiments, one subjects a mass-to-charge-selected parent ion to very low-energy electrons (often boiled off a filament) and then monitors the identities and abundances of the fragment ions generated subsequent to electron capture. In electron-transfer dissociation[5−9] (ETD), one allows the parent ion to undergo collisions with an anion donor (having low electron binding energy, BE_{donor}), which transfers an electron to the parent to produce the fragment ions. Both experiments are usually carried out at or near room temperature. As a result, in ECD the primary source of excess energy is the recombination energy released when the electron is captured, whereas in ETD the available energy is equal to the recombination energy minus the electron binding energy of the anion donor.

In a series of recent papers, we have described our attempts to understand and explain the molecular-level mechanism(s) underlying electron-transfer dissociation (ETD) mass spectrometry. We have suggested that our findings apply as well to electron-capture dissociation (ECD) where free low-energy electrons rather than anion collision partners are used to effect the initial electron attachment to the gaseous parent ion.

The basic questions arising in these studies can be summarized as follows:

(i) When the anion donor A^-, having electron binding energy BE_{donor}, collides with a gas-phase multiply positively charged polypeptide parent ion, to which site(s) in the polypeptide is the electron most likely to be transferred?

(ii) Once the electron attaches to one site, can it transfer to another site in the polypeptide? If so, at what rates and over what distances does this occur?

(1) Zubarev, R. A.; Kelleher, N. L.; McLafferty, F. W. *J. Am. Chem. Soc.* **1998**, *120*, 3265–3266.
(2) Zubarev, R. A.; Kruger, N. A.; Fridriksson, E. K.; Lewis, M. A.; Horn, D. M.; Carpenter, B. K.; McLafferty, F. W. *J. Am. Chem. Soc.* **1999**, *121*, 2857–2862.
(3) Zubarev, R. A.; Horn, D. M.; Fridriksson, E. K.; Kelleher, N. L.; Kruger, N. A.; Lewis, M. A.; Carpenter, B. K.; McLafferty, F. W *Anal. Chem.* **2000**, *72*, 563–573.
(4) Zubarev, R. A.; Haselmann, K. F.; Budnik, B.; Kjeldsen, F.; Jensen, R. *Eur. J. Mass Spectrom.* **2002**, *8*, 337–349.
(5) Syka, J. E. P.; Coon, J. J.; Schroeder, M. J.; Shabanowitz, J.; Hunt, D. F. *Proc. Natl. Acad. Sci. U.S.A.* **2004**, *101*, 9528–9523.
(6) Coon, J. J.; Syka, J. E. P.; Schwartz, J. C.; Shabanowitz, J.; Hunt, D. F. *Int. J. Mass Spectrom.* **2004**, *236*, 33–42.
(7) Pitteri, S. J.; Chrisman, P. A.; McLuckey, S. A. *Anal. Chem.* **2005**, *77*, 5662–5669.
(8) Gunawardena, H. P.; He, M.; Chrisman, P. A.; Pitteri, S. J.; Hogan, J. M.; Hodges, B. D. M.; McLuckey, S. A. *J. Am. Chem. Soc.* **2005**, *127*, 12627–12639.
(9) Gunawardena, H. P.; Gorenstein, L.; Erickson, D. E.; Xia, Y.; McLuckey, S. A *Int. J. Mass. Spectrom.* **2007**, *265*, 130–138.

10.1021/ja100240f

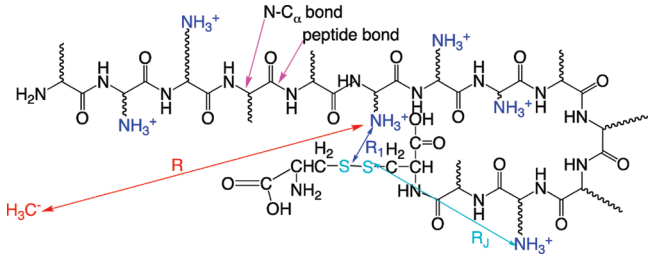

Figure 1. Multiply protonated polypeptide undergoing collision with methyl anion donor showing protonated amine side chains, labeling one SS bond, one peptide bond, and one N−C_α bond. Also shown are distances between the SS bond and some of the positive sites (these distances relate to the Coulomb stabilization at the SS site). Taken from ref 39.

(iii) How does the attached electron cause bonds to break, why are the N−C_α and S−S bonds most common to break in ETD and ECD (but not in other forms of mass spectrometry), and why do these bonds break at many sites throughout the peptide's backbone?

The kinds of systems we have in mind are depicted in Figure 1 where we show an anion donor[10] (the methyl anion in this example) colliding with a polypeptide some of whose side chains are rendered positive by protonation. In this depiction, we also show an example of a peptide bond, an N−C_α bond, and an S−S bond.

1.1. Current View of ETD Mechanism. As a result of theoretical studies on the mechanisms of ETD by several groups, experimental ECD and ETD research by others,[11−39] and adoption of well-established views of ion−molecule and ion−ion reaction mechanisms,[40] the following picture seems to arise:

(i) In the initial ETD anion−cation collision, the anion donor is attracted by strong Coulomb forces toward the positive polypeptide. Most likely, an orbiting anion−cation complex is then formed, as described in a recent paper from the McLuckey group.[10] The radial extent $r_{complex}$ of this orbiting complex depends on the charges Z_C and Z_A of the polypeptide and the donor anion, respectively, as

$$r_{complex} = \frac{2Z_C Z_A}{\mu v^2} \quad (1)$$

where μ is the reduced mass of the anion−cation collision and v is their collision speed. This so-called Thomson model arises from balancing the repulsive centrifugal force with the attractive Coulomb force to obtain an expression for the radius of a stable orbit. The size of the orbit achieved in this initial anion−cation encounter can be very large since the charge Z_C on the parent ion is usually greater than unity and the relative speeds v are small (because ETD is usually carried out at or near room temperature). For example, thermal collisions at $T = 300$ K, produce $r_{complex}$ values of ca. Z_C Z_A 1000 Å. This model results in predicted overall reaction cross sections that scale as the square of the parent ion's total charge, as is commonly observed in ECD and ETD.

(ii) After the orbiting collision complex is formed, eccentricity in the ion pair's path allows the cation and anion to periodically approach more closely during each orbit. During any such close approach, various reactive events can take place: electron transfer, proton transfer, ion-pair formation, and chemical reaction. It is only the former event that we focus on in this paper.

(iii) To realize an electron-transfer from the anion donor to one of the parent ion's positive sites, the donor's orbital holding the excess electron and one or more Rydberg orbitals on that positive site must come into close enough proximity to experience strong electronic coupling. Earlier work[18,19,28] from the author's group showed that cross sections for electron transfer to $n = 3$ Rydberg orbitals on positive sites can be large (0.1−20 Å^2 depending on the electron binding strength of the donor).

(iv) It was also found[18−23,25−30] that for SS σ^* or backbone OCN amide π^* orbitals that experience Coulomb stabilization C in excess of 1 or 2.5 eV, respectively, direct electron transfer from the donor anion to either of these orbitals is also possible albeit with cross sections ca. 1−10% of those for transfer to Rydberg orbitals on positive sites. The Coulomb stabilization at any site depends upon the distances R_J from that bond site to all positive sites (of charges Z_J) in the parent polypeptide ion as shown in eq 2.

(10) Some idea of the range of anion donors used in ETD experiments can been seen in Table 2 of ref 8.
(11) Syrstad, E. A.; Turecek, F. *J. Phys. Chem. A* **2001**, *105*, 11144–11155.
(12) Turecek, F.; Syrstad, E. A. *J. Am. Chem. Soc.* **2003**, *125*, 3353–3369.
(13) Turecek, F.; Polasek, M.; Frank, A.; Sadilek, M. *J. Am. Chem. Soc.* **2000**, *122*, 2361–2370.
(14) Syrstad, E. A.; Stephens, D. D; Turecek, F *J. Phys. Chem. A* **2003**, *107*, 115–126.
(15) Turecek, F. *J. Am. Chem. Soc.* **2003**, *125*, 5954–5963.
(16) Syrstad, E. A.; Turecek, F. *Am. Soc. Mass. Spectrom.* **2005**, *16*, 208–224.
(17) Uggerud, E. *Inter. J. Mass. Spectrom.* **2004**, *234*, 45–50.
(18) Anusiewicz, I.; Berdys-Kochanska, J.; Simons, J. *J. Phys. Chem. A* **2005**, *109*, 5801–5813.
(19) Anusiewicz, I.; Berdys-Kochanska, J.; Skurski, P.; Simons, J. *J. Phys. Chem.* **2006**, *A110*, 1261–1266.
(20) Sawicka, A.; Skurski, P.; Hudgins, R. R.; Simons, J. *J. Phys. Chem.* **2003**, *B107*, 13505–13511.
(21) Sobczyk, M.; Skurski, P.; Simons, J. *Adv. Quantum Chem.* **2005**, *48*, 239–251.
(22) Sawicka, A.; Berdys-Kochaska, J.; Skurski, P.; Simons, J. *Int. J. Quantum Chem.* **2005**, *102*, 838–846.
(23) Anusiewicz, I.; Berdys, J.; Sobczyk, M.; Sawicka, A.; Skurski, P.; Simons, J. *J. Phys. Chem.* **2005**, *A109*, 250–258.
(24) Bakken, V.; Helgaker, T.; Uggerud, E. *Eur. J. Mass Spectrom* **2004**, *10*, 625–638.
(25) Skurski, P.; Sobczyk, M.; Jakowski, J.; Simons, J. *Int. J. Mass. Spectrom* **2007**, *265*, 197–212.
(26) Sobczyk, M.; Neff, D.; Simons, J. *Int. J. Mass Spectrom.* **2008**, *269*, 149–164.
(27) Sobczyk, M.; Simons, J. *Int. J. Mass. Spectrom.* **2006**, *253*, 274–280.
(28) Sobczyk, M.; Simons, J. *J. Phys. Chem. B* **2006**, *110*, 7519–7527.
(29) Neff, D.; Sobczyk, M.; Simons, J. *Int. J. Mass Spectrom.* **2008**, *276*, 91–101.
(30) Neff, D.; Simons, J. *Int. J. Mass Spectrom.* **2008**, *277*, 166–174.
(31) Turecek, F.; Chen, X.; Hao, C. *J. Am. Chem. Soc.* **2008**, *130*, 8818–8833.
(32) Chen, X.; Turecek, F. *J. Am. Chem. Soc.* **2006**, *128*, 12520–12530.
(33) Holm, A. I. S.; Larsen, M. K.; Panja, S.; Hvelplund, P.; Brøndsted Nielsen, S.; Leib, R. D.; Donald, W. A.; Williams, E. R.; Hao, C.; Tureèek, F. *Int. J. Mass Spectrom.* **2008**, *276*, 116–126.
(34) Chamot-Rooke, J.; Malosse, C.; Frison, G.; Tureèek, F. *J. Am. Assoc. Mass Spectrom.* **2007**, *18*, 2146–2161.
(35) Fung, Y.M. E.; Chan, T.-W. D. *J. Am. Assoc. Mass Spectrom.* **2005**, *16*, 1523–1535.
(36) Konishi, H.; Yokotake, Y.; Ishibahsia, T. *J. Mass Spectrom. Soc. Jpn.* **2002**, *50*, 229–232.
(37) Holm, A. I. S.; Hvelplund, P.; Kadhane, U.; Larsen, M. K.; Liu, B.; Nielsen, S. B.; Panja, S.; Pedersen, J. M.; Skryudstrup, T.; Støchkel, K.; Williams, E. R.; Worm, E. S. *J. Phys. Chem. A* **2007**, *111*, 9641–9643.
(38) Neff, D.; Simons, J. *J. Phys. Chem A* **2010**, *114*, 1309–1323.
(39) Simons, J. *Chem. Phys. Lett.* **2010**, *484*, 81–95.
(40) A nice overview of these physical events is given in ref 8.

$$C = -14.4\ \text{eV} \sum_{J=1}^{N} \frac{Z_J}{R_J\,(\text{Å})} \qquad (2)$$

(v) After initial electron attachment to a positive site, it is possible for the electron to transfer either (a) to a Rydberg orbital on another positive site or (b) to an SS σ^* or OCN amide π^* orbital that is sufficiently Coulomb stabilized.

(vi) Once an electron enters an SS σ^* orbital, cleavage of the SS bond occurs promptly. If an electron enters an OCN amide π^* orbital, cleavage of the adjacent N−C_α bond can occur by overcoming a small barrier. A driving force for making the N−C_α bonds susceptible to cleavage is the C−N π bond that is formed after this cleavage. The SS and N−C_α bond-cleavage events are illustrated in Scheme 1.

1.2. Limitations Faced by Our Earlier Theoretical Studies. Although much progress has been made, there have been significant limitations experienced in our studies to date. In particular, we have been limited to (i) studying probabilities and cross sections for electron transfer from anion donors into only very low-energy Rydberg orbitals (i.e., those having n quantum numbers of 3 and, with more effort and less accuracy, $n = 4$) on positive sites, and (ii) studying rates of electron transfer into SS σ^* or OCN amide π^* orbitals from $n = 3$ or $n = 4$ Rydberg orbitals on positive sites.

These limitations relate to the smallest electronic couplings $H_{1,2}$ between diabatic states (e.g., Rydberg orbitals on a protonated amine side chain and an SS σ^* or OCN amide π^* orbital) that we could reasonably evaluate using our ab initio quantum chemistry methods. Only for $n = 3$ and $n = 4$ are the couplings large enough that we feel even modestly confident in the reliability of our ab initio approach; for $n > 4$ they are just too small for us to reliably calculate.

The $H_{1,2}$ couplings between (i) an anion donor orbital and an $n = 3$ or $n = 4$ Rydberg orbital, (ii) an anion donor orbital and an SS σ^* or OCN amide π^* orbital, and (iii) an $n = 3$ or $n = 4$ Rydberg orbital and an SS σ^* or OCN amide π^* orbital were found to be between 10 and 300 cm^{-1} for the model systems we studied. These coupling strengths allowed us to reach conclusions about the magnitudes of the cross sections for transfer from an anion donor to an $n = 3$ or $n = 4$ Rydberg orbital or to an SS σ^* or OCN amide π^* orbital. They also allowed us to conclude that electron transfer from an $n = 3$ or $n = 4$ Rydberg orbital to an SS σ^* or OCN amide π^* orbital could occur at rates exceeding 10^{11} s^{-1} over distances of at least 15 Å.

However, we have not been able to employ ab initio methods to estimate the corresponding rates and transfer distances for Rydberg orbitals having $n > 4$; the $H_{1,2}$ values coupling the Rydberg and SS σ^* or OCN amide π^* orbitals are just too small to be so determined. However, we recently introduced a new physical model[38,39] in terms of which we have been able to estimate the Rydberg-to-SS σ^* or OCN amide π^* $H_{1,2}$ couplings for $n > 4$. In this paper, we extend the use of this new model to estimate $H_{1,2}$ values for anion-to-Rydberg orbital couplings. This advance allows us to offer a more complete set of predictions about (i) into which Rydberg orbitals ETD electron transfer is most likely, given the electron binding energy of the anion donor, and (ii) over what distances intramolecular electron transfer can occur and at what rates, subsequent to electron attachment into a particular Rydberg orbital.

In the Section 2, we briefly review the foundations of the model put forth in refs 38 and 39 and summarize its primary predictions relative to Rydberg-to-SS σ^* or -OCN amide π^* orbital electron transfer rates and distances. In Section 3, we extend this model to treat the intermolecular electron transfer event in ETD by estimating the probabilities and cross sections for anion-to-Rydberg orbital electron transfer for $n > 3$ Rydberg states. In Section 4, we summarize the predictions of our model as related to ETD and offer speculation concerning ECD.

2. Review of Our Model for $H_{1,2}$ As Applied Previously to Intramolecular Rydberg-to-Valence Orbital Electron Transfer

2.1. Using ab Initio Data on $n = 3$ Rydberg Levels As a Baseline. We used ab initio methods to evaluate $n = 3$ and $n = 4$ Ry-to-SS σ^* or -OCN amide $H_{1,2}$ couplings in, for example, model compounds containing one S−S bond and one protonated amine site. An example of the kind of data thus obtained in shown in Figure 2, where energies of Rydberg-attached and SS σ^*-attached electronic states are shown as functions of the S−S bond length for the small model compound H_3C-S-S-$(CH_2)_2$-NH_3^+.

The key data extracted from model studies like this are the coupling strengths between the SS σ^*-attached and various Rydberg-attached states as well as knowledge about which Rydberg states are intersected by the SS σ^*-attached state near the equilibrium geometry of the parent ion. For the example shown in Figure 2, it is one of the 3p states and many of the $n = 4$ and 5 states that meet the second condition. The coupling strengths are shown in Figure 2 as $H_{1,2}$ values in cm^{-1}.

As seen in Figure 2, the $H_{1,2}$ values coupling the SS σ^* state to the 3s and 3p Rydberg states are in the 95−216 cm^{-1} range, whereas that for the 4s Rydberg state is much smaller (ca. 8 cm^{-1}). These findings are typical of our studies to date and illustrate why we need to take a different approach to estimate $H_{1,2}$ values for $n > 3$. Even for the largest $n = 3$ $H_{1,2}$ values, the magnitude of $(\pi H_{1,2}^2/(\hbar\mu v|\Delta F|))$ that enters into the Landau–Zener formula was found to be small enough to produce surface-hopping probabilities much less than unity. Here μ is the reduced mass for the SS bond vibration, v is the average speed of vibration of the SS bond, and ΔF is the difference in the SS σ^*-attached and Rydberg-attached surfaces' slopes at the crossing point.

2.2. Distinct Roles of Coulomb Potentials. Before further describing our new model, it is important for the development offered later in this paper to clarify the roles played by internal Coulomb energies in governing the relative energies of the various (i.e., Rydberg-attached, SS σ^*-attached, and amide π^*-attached) states. In the example shown in Figure 2, the energy of the SS σ^*-attached curve relative to the manifold of Rydberg-attached curves depends on the Coulomb stabilization energy C experienced by an electron on the SS site generated by the positively charged protonated amine. For compounds with more methylene units and thus greater distance separating the SS and amine sites, the SS σ^*-attached curve will be shifted to higher relative energies, so the SS bond lengths at which it crosses various Rydberg curves will be shifted outward.

In a multiply positively charged polypeptide, which is more characteristic of ETD parent ions, Coulomb potentials play three important, yet distinct, roles:

(i) As the anion donor approaches the parent ion from afar, it is the *total charge* Z_C of the cation and that Z_A of the anion that govern the attractive Coulomb potential and determine the radius of the orbiting ion pair as discussed earlier.

Scheme 1. Electron Attachment to SS σ^* or OCN π^* Orbital Followed by SS or N−C_α Bond Cleavage

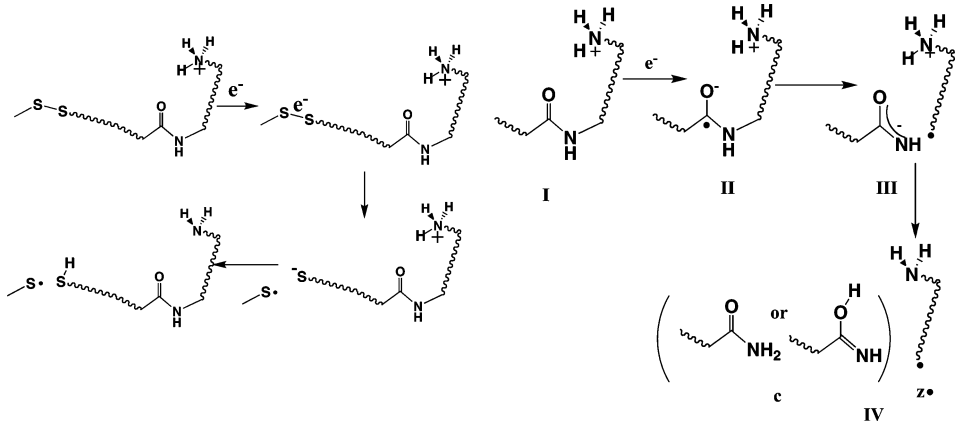

(ii) However, once the anion donor approaches the parent ion more closely (e.g., as in Figure 1), it is the *difference* between the Coulomb potential experienced by the anion and the Coulomb potential existing at each positive site in the parent ion that govern the energy gap between the anion-attached and Rydberg-attached energy surfaces.

(iii) In addition, when considering intramolecular electron transfer, it again is the *difference* between the Coulomb potential at the SS σ^* or amide π^* site and the Coulomb potential existing at each positive site in the parent ion that governs the energy gaps between the SS σ^*- or amide π^* bond-attached and Rydberg-attached energy surfaces.

The *differences* in Coulomb potentials, which enter into the intramolecular electron transfer and the anion-to-cation electron transfer, do not generally depend on the cation's total charge Z_C. For example, when the anion donor approaches closely to any given positive site (e.g., as the methyl anion approaches the protonated amine site shown at the end of the red arrow in Figure 1), that positive site and the anion donor will both be Coulomb stabilized to approximately the same degree by all *other* positive charges in the parent ion. As a result, the *relative energies* of the anion donor-attached and Rydberg-attached (to that positive site) states will depend primarily on the Coulomb energy exerted on the donor-attached state by that *single* positive site nearest the anion. Likewise, if an electron is transferred from a Rydberg orbital on a positive site to a *nearby* SS σ^* or amide π^* orbital, it is (approximately) only the Coulomb potential between that positive site and the SS σ^* or amide π^* bond that governs the relative energies of the Rydberg-attached and SS σ^*- or amide π^*-attached states. For these reasons, when we talk later in this paper about the crossings of anion donor-attached and Rydberg-attached energy surfaces, only the Coulomb interaction of the anion and the single Rydberg site to which the electron is transferred will be considered. It is also for these reasons that data on singly charged model systems such as shown in Figure 2 can be relevant even though in essentially all ETD experiments, the parent ion has multiple positive charges.

2.3. Assumptions Underlying Our New Model. In refs 38 and 39, we introduced simple, but we think reasonable, models for the Rydberg orbitals and for the SS σ^* or OCN π^* orbital, and we made reasonable approximations to cast this model in a form that allows us to estimate rates for $n > 3$ in terms of our ab initio computed rates for $n = 3$. Specifically, in creating our new model, we realized that (i) each Rydberg orbital's radial probability density $P(r)$ is largest within a "shell" of thickness T that peaks near the orbital's average radial extent $r \approx \langle r \rangle$ and decays exponentially at larger r and (ii) each Rydberg orbital

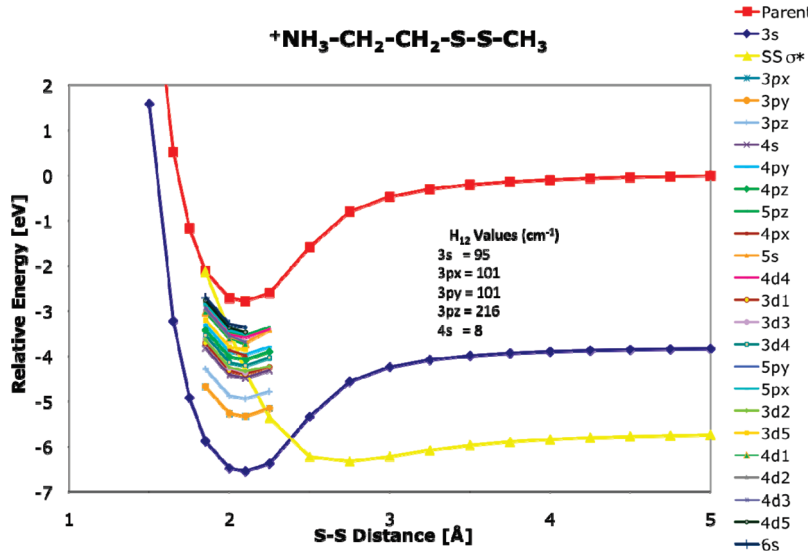

Figure 2. Energies as functions of SS bond length for H_3C-SS-$(CH_2)_2$-NH_3^+ parent ion as well as SS σ^*-attached and various Rydberg-attached species. Taken from ref 38.

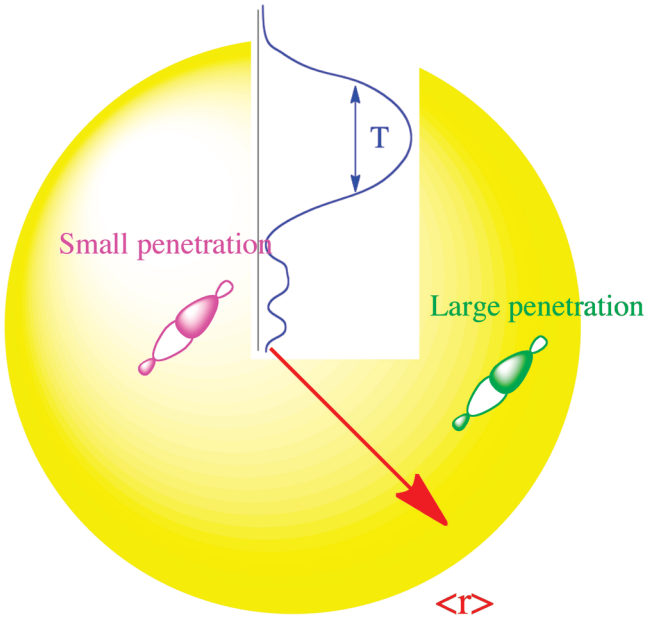

Figure 3. Qualitative depiction of a 3s Rydberg orbital having radial size <*r*> and thickness *T* showing a valence orbital placed to give large or small (being too close and thus outside the major radial shell) penetration with the Rydberg orbital. Also shown are the large peak in the radial density and the smaller inner-shell peaks.

has smaller inner-shell peaks at smaller *r* values, but we assumed its coupling with a valence-sized orbital (i.e., the SS σ^* or OCN amide orbital) will be largest when the valence orbital is localized within the major shell of the Rydberg orbital, thus achieving what we termed *large penetration* of the valence and Rydberg orbitals.

In Figure 3 we show a qualitative depiction of a 3s Rydberg orbital within which an SS σ^* orbital is placed (i) in the Rydberg orbital's radial shell of large amplitude (so penetration is large) or (ii) too close to the Rydberg orbital's center (so penetration is small). This assumption that the valence and Rydberg orbitals must lie within a critical range of distances and *neither too close nor too distant* plays a key role in the model we introduced. It is well-known and obvious that poor coupling will occur if the valence and Rydberg orbitals are too far from one another since both orbitals decay exponentially with distance.[8] However, the postulate that poor coupling will also occur if the valence orbital is too close to lie within the Rydberg orbital's major shell is new to our model, although there is some recent experimental data from the Williams[41] group that seem to support this claim.

The radial probability density of this 3s Rydberg orbital is shown in blue in Figure 3, where the two radial nodes associated with the 3s orbital and the inner-shell lesser peaks are also shown. More quantitative depictions of 3s, 3p, 3d, 4s, 4p, and 5s Rydberg orbitals are shown in Figure 4 where SS σ^* orbitals having large penetration to several are shown in green. Note that the Rydberg orbitals are shown in Figure 4 with sizes reflecting only 60% of their electron density inside their outermost contour; their 90% contours would display them as even larger sizes.

Although these Rydberg orbitals have varying numbers of radial nodes, they all have a radial shell of highest probability density near their outermost regions.

(41) Prell, J. S.; O'Brien, J. T.; Holm, A. I. S.; Lieb, R. D.; Donald, W. A.; Williams, E. R. *J. Am. Chem. Soc.* **2008**, *130*, 12680–12689.

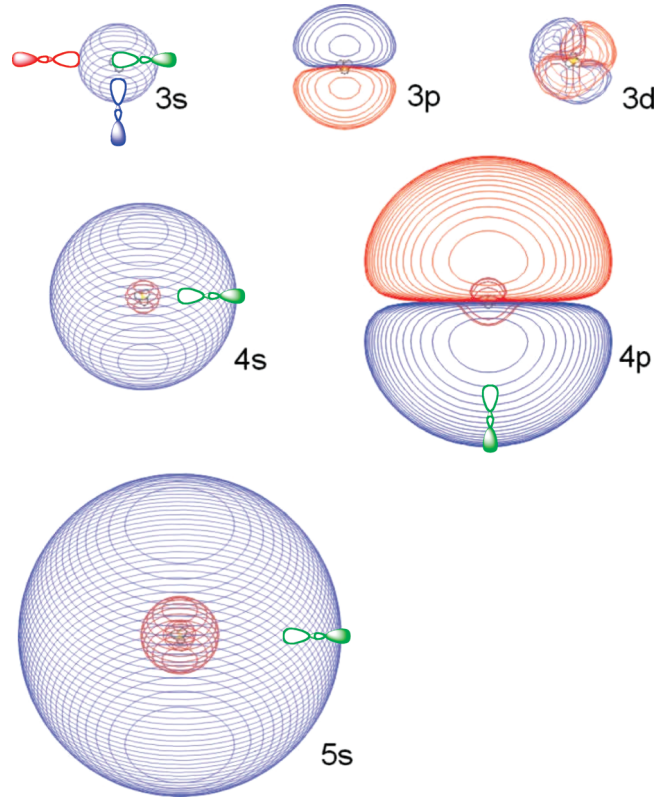

Figure 4. Rydberg orbitals shown with their outermost contour containing 60% of their total electron density to illustrate their varying sizes. Also shown in green are valence-sized orbitals placed to achieve large penetration with the Rydberg orbitals' major radial shell. Taken from ref 39.

2.4. Radial-Shell Approximation. Further assumptions used in creating the model introduced in refs 38 and 39 include:

(iii) We approximated the probability density of each Rydberg orbital in terms of uniform density within its spherical shell of radius <*r*> and thickness *T* (and thus volume $V_n = 4\pi<r>^2T$) with these size parameters given in terms of the Rydberg orbital's *n* quantum number as follows:

$$<r> = \frac{n(n + 1/2)a_0}{Z} \tag{3a}$$

and

$$T = \sqrt{<r^2> - <r>^2} = \frac{na_0}{Z}\frac{\sqrt{n + 1/2}}{\sqrt{2}} \tag{3b}$$

These approximations arise from describing the Rydberg orbital's major amplitude in hydrogenic form $r^{n-1}\exp(-Zr/na_0)$, where a_0 is the Bohr radius. Although the derivation in refs 38 and 39 is based on using this s-orbital hydrogen form, as we discuss later, the results likely offer guidance for Rydberg orbitals having nonzero angular momentum. After all, such Rydberg orbitals differ primarily in the number of inner-shell radial nodes they possess (and these play no role in our theory) and in their directional character (which we treat later in this derivation).

So, each Rydberg orbital ψ_n is approximated as being constant within its orbital volume V_n:

$$\psi_n = (1/V_n)^{1/2} = (4\pi < r>^2T)^{-1/2} \tag{4}$$

where <*r*> and *T* depend on *n* as shown in eqs 3a and 3b. The SS σ^* or OCN π^* orbitals were also approximated by a function of uniform amplitude within a volume V_{bond} of valence-orbital size:

$$\psi_{bond} = (1/V_{bond})^{1/2} \quad (5)$$

where the volume of this orbital $V_{bond} = 4/3\pi x^3 a^3_0$ in cubic Bohrs is expressed in terms of a dimensionless parameter *x*.

One might wonder why the nodal character of the SS σ^* or OCN π^* orbital is not essential to consider in constructing this model. The reason is that it is not the overlap integral, which would involve the signs of the SS σ^* or OCN π^* and Rydberg orbitals, that is most related to the electronic coupling $H_{1,2}$. Rather, in $H_{1,2}$ one also has all of the electron−nuclear attraction potentials, the electronic kinetic energy operator, and the electron−electron repulsions. The sum of all of these operators does not commute with symmetry operators that describe the local nodal symmetry of the SS σ^* or OCN π^* and Rydberg orbitals, so $H_{1,2}$ will not vanish even when the overlap integral does.

(iv) We assumed the $H_{1,2}$ coupling strengths to be proportional to the penetration integral *S* given by the product of the SS σ^* or OCN π^* orbital ψ_{bond} and the Rydberg orbital ψ_n integrated over the volume V_{bond} that they share:

$$S = \int_{V_{bond}} \frac{1}{V_{bond}^{1/2}} \frac{1}{V_n^{1/2}} d^3r = \frac{V_{bond}^{1/2}}{V_n^{1/2}} = \sqrt{\frac{2x^3Z^3}{3n^3\left(n+\frac{1}{2}\right)^2\sqrt{2n+1}}} \quad (6)$$

It is the analytical form of the *n*-dependence in eq 6 that allows us to express the *n*-dependence of $H_{1,2}$ and thus of the rates.

(v) Finally, we assumed the rate of Rydberg-to-SS σ^* or -OCN π^* orbital electron transfer is proportional to the square of $H_{1,2}$ as the Landau−Zener formula we used to compute the rates for $n = 3$ suggests.

2.5. Relating Intramolecular Transfer Rates for $n > 3$ to ab Initio Rates for $n = 3$. The ab initio computed rate of electron transfer for the 3s Rydberg orbital case was estimated by multiplying the frequency ν at which the Rydberg and SS σ^* (or amide π^* N−C_a) surfaces cross (taken to be approximately the SS or N−C vibrational frequency) by the Landau−Zener estimate of the probability *P* that intramolecular electron transfer takes place. This produced a rate of ca. 10^{12} s^{-1} for the 3s-Rydberg orbital case. Using this ab initio calculated rate and employing the model described above to estimate the *n*-dependence of the $H_{1,2}$ couplings, we were able to express the rates of Rydberg-to-SS σ^* or -OCN π^* orbital electron transfer for $n > 3$ in terms of the ab initio $n = 3$ rates as follows:

$$\text{rate}_n = \frac{3^3(3+1/2)^{5/2}}{n^3(n+1/2)^{5/2}} \times 10^{12}\ s^{-1} \quad (7)$$

In the Landau−Zener formula used to derive eq 7 the surface-slope difference ΔF and the speed υ of passing through the surface crossing appear along with $H_{1,2}$. However, as can be see from Figure 2: (i) At the surface crossings, the slope differences pertinent to the SS σ^* and all of the Rydberg curves are very similar, especially when one considers that only crossings at geometries near the equilibrium geometry of the parent ion (i.e., near the minima of the Rydberg curves) can be accessed by thermal vibrational motion (and are thus pertinent).

Table 1. Radial Size <*r*>, Thickness *T*, and Maximum Electron Transfer Rates (eq 7) for Transfer from Rydberg Orbitals of Various Principal Quantum Number *n* to a Valence SS σ^* or OCN π^* Orbital

principal quantum number *n*	radial size[a] <*r*> (Å) for $Z = 1$	thickness *T* (Å) for $Z = 1$	$\frac{3^3(3+1/2)^{5/2}}{n^3(n+1/2)^{5/2}}$	maximum rate s^{-1} for $Z = 1$
3	5.5	2.1	1	10^{12}
4	9.5	3.2	0.225	2×10^{11}
5	14.5	4.4	0.070	7×10^{10}
6	20.6	5.7	0.027	3×10^{10}
7	27.8	7.2	0.012	1×10^{10}
8	36.0	8.7	0.006	6×10^{9}
10	55.5	12	0.002	2×10^{9}
20	217	34	4×10^{-5}	4×10^{7}

[a] According to eqs 3a and 3b, <*r*> and *T* should scale with *Z* as Z^{-1}.

(ii) The vibrational speed υ associated with each surface crossing is determined by the SS bond's vibrational energy $1/2\mu\upsilon^2$ and thus should be similar if, by assumption, the Rydberg curves must be crossed near their minima where the SS bond has little if any excess vibrational energy.

For these reasons, the ΔF and υ factors can be ignored and the ratios of rates can be taken to be proportional to the ratios of the squares of the $H_{1,2}$ values, and this is how the approximation in eq 7 was obtained.

It is important to emphasize that eq 7 gives us an expression for how the $H_{1,2}$ values depend upon *n*, not how the $H_{1,2}$ value for a particular *n* depends upon distance. In ref 8, McLuckey and co-workers described a model for the distance dependence of $H_{1,2}$ for a *given* Rydberg state and for a specified BE_{donor}. Their model shows the expected exponential decay with distance that arises from the exponential asymptotic forms of the Rydberg and anion-donor orbitals. Our model focuses, for any particular distance between the Rydberg and SS σ^* or OCN π^* orbital (and later for any distance between the Rydberg and anion donor orbitals), on the specific Rydberg orbital having the size <*r*> and thickness *T* to span that distance. As the distance varies, in our model, the special Rydberg orbital that has the correct <*r*> and *T* varies, and it is this variation that eq 7 describes.

2.6. Results for Intramolecular Electron Transfer Rates and Distances. In Table 1, for values of *n* ranging from 4 to 20, we show the estimated rates obtained from eq 7 as well as the size <*r*> and thickness *T* belonging to each orbital.

The rate predictions (it is important to note that experimental testing of these predictions is still needed) shown in Table 1 are important because they contribute to our understanding of ETD's mechanism.

(i) Our earlier findings suggest that the initial electron transfer takes place between the anion donor and a positively charged site (i.e., into a Rydberg orbital) rather than directly into an SS σ^* or OCN π^* orbital, so we will focus on what happens after an electron is captured into a Rydberg orbital.

(ii) Earlier studies by others[42] concluded that excited Rydberg states undergo radiative or radiationless relaxation to lower-energy Rydberg states at rates of ca. 10^6 s^{-1}. However, once the ground $n = 3$ Rydberg level is reached, this cascade terminates and, for example, the protonated amine site falls apart into either -NH_2 + H or NH_3 plus a carbon radical at rates that can exceed 10^{11} s^{-1}.

(42) Excited Rydberg states are known to undergo a cascade of radiationless or radiative relaxation events to lower-energy Rydberg levels on time scales of ca. 10^{-6} s per transition. See, for example: Turecek, F.; Reid, P. J. *Int. J. Mass Spectrom.* **2003**, *222*, 49–61.

(iii) As seen in Table 1, our model predicts that Rydberg states with $n < 10$, if populated in the initial ETD event, will *not* decay to lower-energy Rydberg levels. Instead, they will be kinetically favored to undergo electron transfer to any SS σ^* or OCN π^* orbital that is within $\langle r \rangle \pm T/2$ of the Rydberg site (if that SS σ^* or OCN π^* orbital is sufficiently Coulomb stabilized) at rates exceeding the relaxation rate of 10^6 s^{-1}. Valence orbitals that lie outside this distance range (*too far or too close*) will not participate.

(iv) As also seen in Table 1, the distances over which such electron transfer can occur can be as large as ca. 50 Å (for $n = 10$), but only if such high-n states are populated.

(v) Only Rydberg states with $n > 20$, if populated in the initial ETD event, would be expected to relax to lower-energy Rydberg levels. Upon reaching $n \approx 10-20$, the electron transfer rate will exceed the rate of further relaxation within the Rydberg manifold.

(vi) For each Rydberg orbital, there is a limited range of distances over which electron transfer is expected. For example, for $n = 3$, this range ($\langle r \rangle \pm T/2$) is from 4.5 to 6 Å, and for $n = 4$ it is from 8 to 11 Å. Being either *too far or too close* causes the transfer rate to decay.

(vii) If an $n = 3$ Rydberg state is populated in the initial ETD event, it can transfer an electron to a Coulomb-stabilized SS σ^* or OCN π^* orbital over a distance of 4.5−6 Å (if such an orbital is located within this range) and at a rate of ca. 10^{12} s^{-1}, but it can also decay to -NH_2 + H or NH_3 plus a carbon radical.

It should be noted that the n-dependence of the intramolecular electron transfer rates derived from eq 7 and reflected in Table 1 is not in quantitative agreement with the ab initio $H_{1,2}$ values for $n = 3$ and $n = 4$ shown in Figure 2 for SS bond cleavage. In Table 1, the $n = 4$ rates are estimated to be ca. 20% of the $n = 3$ rates, although the $n = 4$ ab initio $H_{1,2}$ value in Figure 2 is 10% of the $n = 3$ ab initio $H_{1,2}$ value (suggesting the $n = 4$ rate should be only 1% of the $n = 3$ rate). However, it is our belief that the $n = 4$ ab initio $H_{1,2}$ data are not sufficiently reliable (i.e., 8 cm^{-1} is just too small an energy to extract from our data) to conclude that this observation casts serious doubts on the model embodied in eq 7. In other words, we trust the model more than we do the $n = 4$ ab initio $H_{1,2}$ values.

This now brings us to what the present paper is about. Although the new model we put forth allows us to estimate rates and distances of *intermolecular* Rydberg-to-SS σ^* or -OCN π^* orbital electron transfer, *we still need to know which Rydberg level(s) the initial ETD event can populate and with what probabilities*. As mentioned earlier, our ab initio studies allowed us to estimate cross sections for ETD attachment to $n = 3$ Rydberg levels, but we need an approach to estimate the cross sections for levels with $n > 3$.

3. Application of Our Model to Anion Donor-to-Rydberg ETD Electron Transfer

The electron biding energy of the anion donor, BE_{donor}, places limits on the highest Rydberg level that can be populated. Specifically, only Rydberg levels having binding energies in excess of the donor's binding energy can be accessed in the ETD process:

$$-E(n) > BE_{donor} \tag{8}$$

The ground (i.e., 3s) Rydberg levels for protonated and fixed-charge side chains have energies in the range of −4 to −2 eV, respectively, and excited Rydberg levels have smaller binding energies that can be expected to be approximated by the well-known Rydberg energy formula for any value of n.

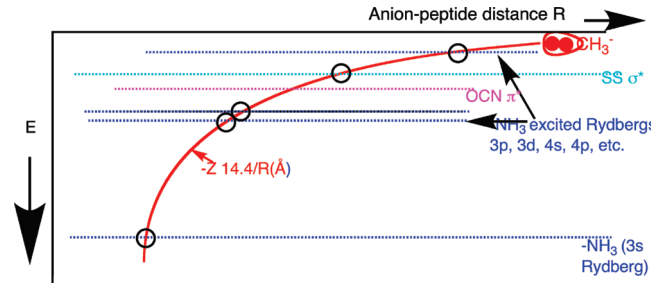

Figure 5. Qualitative depictions of the entrance-channel ion-pair state and those states in which the excess electron has transferred to the ground- or excited-Rydberg orbital or to an SS σ^* or OCN π^* orbital. Taken from ref 39.

3.1. Surface-Crossing Condition. According to the Landau–Zener view of collisional electron transfer, the transfer to a Rydberg level having energy $E(n)$ will be most facile when the diabatic electronic energy surface of the anion-polypeptide complex crosses that of the state in which the donor is rendered neutral and its excess electron resides in the n^{th} Rydberg state. (The zero of energy is taken to correspond to the parent polypeptide and the anion donor, with its electron removed, infinitely far from one another. So, all of the Rydberg levels have energies below zero as does the anion donor whose energy is $-BE_{donor}$.) This condition can be expressed as follows:

$$-\frac{14.4Z\ \text{eV}}{R_C\ (\text{Å})} - BE_{donor} = E(n) \tag{9}$$

where R_C is the distance between the parent polypeptide and the anion donor at which the surface crossing occurs. As discussed earlier, the Coulomb interaction between the anion donor and the parent cation at very long distances depends on the total charge Z_C of the cation. However, once the donor is close enough to transfer an electron to a Rydberg orbital residing on a positive site, the two sites will experience approximately the same Coulomb interactions with all the *other* charges in the system. So, it is only the mutual Coulomb potential between the anion donor and the specific Rydberg site to which electron transfer is taking place that will govern the relative energies of these two states. For this reason, the factor Z in eq 9 should be interpreted not as the total charge Z_C of the parent ion but as the product of the charges on the donor anion and on the site to which the electron is transferred. Often, Z will be unity.

The left side of eq 9 describes the behavior of the ion-pair state of the reactant anion−cation collision; $-BE_{donor}$ is its value at $R \rightarrow \infty$, and the other term is the Coulomb potential acting between the two oppositely charged ions. The right side is simply the energy of the neutralized donor with the excess electron in the nth Rydberg state.

In Figure 5 we show a qualitative depiction of the entrance-channel ion-pair surface as well as surfaces with the excess electron transferred to various Rydberg levels or to a Coulomb-stabilized SS σ^* or OCN π^* orbital all as functions of the anion−cation separation denoted R.

Assuming that the surfaces of all states but the ion-pair state are weakly varying with R in the crossing regions (this is likely a good approximation if the crossing points occur at large anion−cation separations), one can estimate the separation at which the ion-pair and Rydberg states will occur from eq 9:

$$R_C = \frac{14.4Z}{-BE_{donor} - E(n)} \quad (10)$$

For example, for a 3s Rydberg level having $E(3) = -3.5$ eV, R_C ranges from 4 Å (for BE_{donor} near zero) to larger distances as BE_{donor} increases. A 4s Rydberg level having $E(4) = -1.5$ eV has $R_C = 9.6$ Å (for BE_{donor} near zero) or larger. So, except for transfer into the lowest Rydberg orbitals, the surface crossing distances are considerably larger than distances within which chemical bonds or hydrogen bonds are dominant. However, these surface-crossing distances are much smaller than the orbiting-collision radius (i.e., >1000 Å for thermal collisions as expressed in the Thomson model discussed earlier) arising in the initial anion−cation collision event.

3.2. Landau−Zener Surface-Hopping Probabilities. The Landau−Zener formula

$$P = 1 - \exp\left[-\frac{2\pi H_{1,2}^2}{\hbar v|\Delta F|}\right] \approx \frac{2\pi H_{1,2}^2}{\hbar v|\Delta F|} \quad (11)$$

expressing the probability P of a hop from the ion-pair surface onto a Rydberg-attached surface contains the $H_{1,2}$ coupling between the anion donor and Rydberg orbital, the anion−cation relative speed v with which the surface crossing is reached, and the difference in slope $|\Delta F|$ between the ion-pair and Rydberg-attached surfaces at the crossing point. $|\Delta F|$ and v can be approximated on the basis of eq 9 as follows:

$$|\Delta F| = \frac{(-E(n) - BE_{donor})^2}{14.4Z}\frac{eV}{Å} \quad (12)$$

$$v = \sqrt{\frac{2}{\mu}(-E(n) - BE_{donor})} \quad (13)$$

In writing eq 13, we assume that the (thermal) cation−anion relative speed at very large-R can be neglected. This is especially valid for Rydberg states whose crossings occur at low energy; for them, the Coulomb energy drop greatly exceeds the initial thermal collision energy (at least in typical ETD experiments). Unlike the situation discussed earlier in which electron transfer from a Rydberg orbital to an SS or OCN orbital occurs, the ΔF and v factors appearing in eqs 12 and 13 must be explicitly evaluated because they vary significantly from one transition to another. The linearized approximation given on the far right side of eq 11 will be used in our subsequent analysis because we will see that the hopping probabilities P will be considerably less than unity.

In principle, eqs 11−13 allow us to estimate the probability for populating a given Rydberg level if we know the anion binding energy, the energy-level pattern of the Rydberg levels, and the coupling matrix element $H_{1,2}$. We can then estimate the cross section σ for electron transfer into that Rydberg level by

$$\sigma = 2P(1 - P)\pi R_C^2 \approx 2P\pi R_C^2 \quad (14)$$

There are two issues that stand in our way: (i) we need to have an analytical expression for $H_{1,2}$ for $n > 3$ (this will be obtained shortly), and (ii) we need to keep in mind that, according to our model, the anion-to-Rydberg separation R_C at which surface crossing occurs (eq 10) needs to lie within the $\langle r\rangle \pm T/2$ range of that Rydberg orbital for $H_{1,2}$ to be non-negligible. We emphasize that it is the combination of these two conditions that plays a key role in our model.

Table 2. Surface-Crossing Distances R_C (Å) from eq 10 for Various Combinations of Rydberg Energy Levels $E(n)$ and Anion Donor Binding Energy BE_{donor}[a]

<r> ± T/2 Å	n	-E(n) eV	BE_{donor} 2.5 eV	2.0	1.5	1.0	0.5	0.1	0.0
4-7	3	4.0	9.6	7.2	5.8	4.8	4.1	*3.7*	*3.6*
4-7	3	3.5	14.4	*9.6*	7.2	5.8	4.8	4.2	4.1
4-7	3	3.0	28.8	14.4	*9.6*	7.2	5.8	5.0	4.8
4-7	3	2.5		28.8	14.4	*9.6*	7.2	6.0	5.8
4-7	3	2.0			28.8	14.4	*9.6*	7.6	7.2
8-11	4	1.5				28.8	*14.4*	10.3	9.6
8-17	4-5	1.0					28.8	16.0	14.4
17-31	6-7	0.5						*36*	28.8
24-31	7	0.4						48	*36*
24-40	7-8	0.3						72	*48*
32-50	8-9	0.2						144	72
40-61	9-10	0.1							144

[a] For each $E(n)$, the value of n most likely to correspond is also shown as is the value of $\langle r\rangle \pm T/2$ (Å). The $n = 3$ levels for protonated and fixed-charge sites have energies ranging from near −4 eV to near −2 eV, so we included this range in assigning the label $n = 3$. In red are R_C values lying within $\langle r\rangle \pm T/2$; in black *italic* are those close to $\langle r\rangle \pm T/2$; the remainder in black are those lying outside $\langle r\rangle \pm T/2$.

3.3. Importance of the Surface-Crossing and Large-Penetration Conditions. The requirements that the anion-Rydberg separation distance obey the curve-crossing condition eq 10 for a particular Rydberg orbital and lie within the same Rydberg orbital's shell $r \approx \langle r\rangle \pm T/2$ severely limit the Rydberg levels that will be preferentially populated. To illustrate the restrictions arising from these two constraints, we show in Table 2 the surface-crossing distances R_C for various combinations of $E(n)$ and BE_{donor}, over ranges that are representative of Rydberg orbital energies (e.g., for protonated and fixed-charge side chains) and for anion donors commonly used in ETD. We also show the values of n most likely related to each $E(n)$ as well as the $\langle r\rangle \pm T/2$ ranges associated with each n. The empty cells in Table 2 correspond to cases in which BE_{donor} is too large to access the Rydberg level.

At first glance, the trends seen in Table 2 seem rather clear. Donors with large BE_{donor} values populate only low-energy Rydberg levels, while donors with smaller BE_{donor} values can populate a wider range of Rydberg levels. However, this view reflects only the surface-crossing condition that must be obeyed for electron transfer to be facile. It is very important to also consider the large-penetration condition before reaching conclusions about which states will be most populated.

In Table 2, we used red symbols to denote those surface-crossing distances that also lie within the $\langle r\rangle \pm T/2$ range of the pertinent Rydberg level and thus describe ETD events meeting *both* the energy-resonance and large-penetration conditions. In italic font, we labeled distances that we judge to be close to meeting these criteria. The most important conclusions to reach from the data in Table 2 are

(i) Rydberg levels above 8 or 9 do not have surface-crossing distances lying within their $\langle r\rangle \pm T/2$ shell thickness for any value of BE_{donor}, so the model predicts that such levels are unlikely to be populated even by donors of very low binding energy.

(ii) Rydberg levels between 3 and 8 can be accessed, but high values of BD_{donor} can only populate low-n levels, whereas low values of BD_{donor} can populate low-n and higher-n levels.

(iii) So, we expect ETD to populate $n = 3$ (for donors of any BD_{donor}) and levels up to only ca. $n = 8$ (for donors with very small BD_{donor}). The $n = 3$ Rydberg level can produce H atoms (via N−H bond cleavage) or NH_3 (via C−N bond cleavage) or electron transfer to nearby (4.5−6 Å distant) SS

σ^* or OCN π^* orbitals. The $n > 3$ levels can transfer an electron to more distant SS σ^* or OCN π^* orbitals.

The first two of these observations are similar to those made in ref 8 from the McLuckey group. Because the anion donors used in most ETD experiments have BE_{donor} values in the range covered in Table 2 and because the $3 \le n < 10$ Rydberg energies of protonated and fixed-charge sites fall within the energy range in Table 2, we suggest that the above conclusions should be generally valid for ETD. It should be noted that issues such as Franck−Condon factors, which McLucky has shown can have substantial effects, are not being considered in this work. Our model deals only with orbital overlap effects.

The constraints relating BE_{donor} and the n-values that can be accessed in ETD are important to be aware of, but we still need to have a way to estimate the rates for those events that Table 2 shows are expected to occur (i.e., those in red and italic). Our approach to addressing this issue is to derive an expression for the ratio of the surface-hopping probability $P(n)$ for populating an s-type Rydberg orbital having quantum number $n > 3$ to the ab initio calculated probability $P(3)$ that we obtained applying Landau−Zener theory to the crossing of ion-pair and 3s Rydberg-attached diabatic states.

3.4. Relating 3s Surface-Hopping Probabilities to $n > 3$ Probabilities. Starting with eq 11, we can express the surface-hopping probability ratio as

$$\frac{P(n)}{P(3)} = \frac{1 - \exp\left[-\frac{2\pi H_{1,2}^2}{\hbar v|\Delta F|}\right]_n}{1 - \exp\left[-\frac{2\pi H_{1,2}^2}{\hbar v|\Delta F|}\right]_3} \approx \frac{\left(\frac{H_{1,2}^2}{v|\Delta F|}\right)_n}{\left(\frac{H_{1,2}^2}{v|\Delta F|}\right)_3} \quad (15)$$

We use the linearized Landau−Zener expression because, as stated earlier, the ab initio hopping probabilities $P(3)$ and the $P(n)$ we derive here are all significantly less than unity. Specifically, $P(3)$ for electron transfer from H_3C^- to the 3s Rydberg orbital on a protonated site were found to be in the 10^{-2} to 10^{-3} range in our earlier ab initio studies. Now, using eqs 12 and 13 as well as making use of eq 6 to relate $H_{1,2}$ to S and thus to n, we obtain

$$\frac{P(n)}{P(3)} = \left(\frac{-E(3) - BE_{donor}}{-E(n) - BE_{donor}}\right)^{5/2} \frac{3^3(3 + 1/2)^{5/2}}{n^3(n + 1/2)^{5/2}} = [\text{slope} - \text{speed}] \times H_{1,2}^2 \quad (16)$$

The first factors on the right side of eq 16 arise from the slope ΔF- and speed v-dependence, and the second factors arise from the n-dependence of $H_{1,2}^2$ as discussed earlier (see eq 6).

In Table 3 we show, for various values of $E(n)$ and BE_{donor}, both eq 16's slope-speed and $H_{1,2}^2$ contributions to the ratio $P(n)/P(3)$, but only for cases that meet *both* the curve-crossing and large-penetration conditions. Clearly, the values of $P(n)/P(3)$ shown in red in Table 3, formed by taking the product of the two contributions of eq 16, are of similar magnitudes for all values of BE_{donor} and $E(n)$ and range from 1 to ca. 6. Keeping in mind that $P(3)$ was found in our ab initio calculations to be 10^{-3} to 10^{-2}, the $P(n)/P(3)$ ratios shown in red in Table 3 suggest that all of the $P(n)$ (at least for the reasonable $E(n)$ and BE_{donor} values assumed) will lie in the 10^{-3} to 10^{-1} range. Most importantly, these data suggest the $P(n)$ for all Rydberg levels that meet the surface-crossing and large-penetration criteria discussed earlier will be within an order of magnitude of $P(3)$.

Table 3. Slope and Speed Ratios (in Black Bold and Black Italic) for Various $E(n)$ and BE_{donor} Combinations[a]

$H_{1,2}^2$ ratio[b]	n	-E(n) eV	BE_{donor} 2.5 eV	2.0	1.5	1.0	0.5	0.1	0.0	(n/3)[c]
1	3	3.5		*1*	**1**	**1**	**1**	**1**	**1**	**1**
0.225	4	1.5					*16/3.6*	**9/2**	**8/2**	**1.3**
0.225-0.070	4-5	1.0						**28/6-2**	**23/5-2**	**1.3-1.7**
0.027-0.012	6-7	0.5					*211/6-3*	**130/4-2**		**2-2.3**
0.012	7	0.4							*226/3*	**2.3**
0.012-0.006	7-8	0.3							*464/6-3*	**2.3-2.7**
0.006-0.003	8-9	0.2								
0.003-0.002	9-10	0.1								

[a] In the left column are the $H_{1,2}^2$ ratios for each n corresponding to a given $E(n)$. In red are shown the total probability ratios obtained from eq 16 by multiplying together the slope-speed and $H_{1,2}^2$ contributions. For $n > 3$, the values are calculated as $((-E(3) - BE_{donor})/(-E(n) - BE_{donor}))^{5/2}$using the value $E(3) = -3.5$ eV typical for protonated sites. In italic are shown values for cases where R_C is close to lying within $<r> \pm T/2$. In bold are shown values for cases where R_C is within $<r> \pm T/2$. [b] Evaluated as $(3^3(3 + 1/2)^{5/2})/(n^3(n + 1/2)^{5/2})$ for the n-values shown in the second column. [c] These degeneracy factors are explained in Section 3.5.

3.5. Rydberg Orbitals with Nonspherical Shape. As discussed earlier, the derivation resulting in eq 16 was based on treating the Rydberg orbitals as having s-symmetry. To estimate the $P(n)$ for Rydberg orbitals having nonzero orbital angular momentum L, we can proceed as follows:

(i) Although Rydberg orbitals with $L > 0$ have different numbers of inner-shell peaks and radial nodes, they still possess a dominant major peak near $r = <r>$, so we propose it is still reasonable to describe their radial probability density as we did for the s-symmetry orbitals in terms of a single radial shell of radius $<r>$ and thickness T.

(ii) Within each group of Rydberg orbitals having a specific L-value, one orbital will have angular character to optimally direct it toward the incoming anion donor. For example, if we use the anion-to-cation distance vector to define the z-axis, the p(z) or $d(z^2)$ Rydberg orbitals will have major lobes positioned to offer large penetration to the anion donor's orbital, but the p(y), p(x), d(xy), d(xz), $d(x^2-y^2)$, and d(yz) will not. In fact, for each n-value, there will be n Rydberg orbitals that can offer large penetration opportunity. For $n = 3$, it is 3s, 3p(z), and $3d(z^2)$; for $n = 4$ it is 4s, 4p(z), $4d(z^2)$, and $4f(z^3)$, and so on.

(iii) Although we computed the surface hopping probability using ab initio tools for only the 3s Rydberg orbital, the model offered here suggests that nearly the same values will pertain to the 3p(z) and $3d(z^2)$ orbitals. That is, the probability for hopping onto any well-aligned $n = 3$ Rydberg level is postulated to be the same. So, the total probability of accessing the set of $n = 3$ Rydberg orbitals will be three times the values of $P(3)$ that quote above in Table 3.

Therefore, to account for higher-L Rydberg orbitals within the model embodied in eq 16, one should correct the $P(n)/P(3)$ ratios shown in red in Table 3 by multiplying them by the degeneracy factor $n/3$ given in the right-most column in Table 3. The $n/3$ quantity is the number of well-aligned Rydberg orbitals belonging to quantum number n relative to the three orbitals belonging to $n = 3$. However, as explained above, we now have to interpret $P(3)$ as the combined probability for populating the set of 3s, 3p(z), and $3d(z^2)$ orbitals. Even after making these corrections to the data shown in red in Table 3, *we conclude that the P(n)n/3 values are expected to be 1−15 times P(3)* for all of the Rydberg levels that meet the energy-resonance and large-penetration criteria (recall that $P(3)$ was found to be between 10^{-3} and 10^{-2}).

The bottom line is that the combination of surface-crossing and large-penetration conditions constrain n to be between 3 and 7 or 8 (Table 2), and the probabilities expected for ETD

Table 4. n$P(n)$/(3P(3)) and $R^2_C(n)/R^2_C(3)$ Contributions to ETD Cross Sections[a] Relative to the $n = 3$ Cross Section ($3 \times 10^{-2} - 3 \times 10^{-1}$ Å^2) for Those Transitions That Obey Both the Surface-Crossing and Large-Penetration Criteria

<r> ± T/2 Å	n	-E(n) eV	BE_{donor}	2.0	1.5	1.0	0.5	0.1	0.0
4-7	3	3.5		*1*	**1**	**1**	**1**	**1**	**1**
8-11	4	1.5					*5/9*	**3/6**	**3/5**
8-17	4-5	1.0						**10-3/14**	**9-3/12**
17-31	6-7	0.5						*14-16/72*	**9-4/49**
24-31	7	0.4							*7/77*
24-40	7-8	0.3							*16-5/136*

[a] In purple are shown the values of (n$P(n)$)/(3P(3)). In red are shown the values of $[-E(3) - BE_{donor}]^2/[-E(n) - BE_{donor}]^2$ obtained using $E(3) = -3.5$ eV. The cross sections, relative to the cross section for populating all three well-aligned $n = 3$ Rydberg levels are evaluated by multiplying the purple and red numbers in each cell.

into Rydberg orbitals having n between 4 and 7 or 8 are 1−15 times the probability for attaching to the $n = 3$ Rydberg level.

3.6. Cross Sections for $n > 3$ Related to Those for $n = 3$. With the above estimates of $P(n)/P(3)(n/3)$ in hand, we can now estimate the cross sections for populating all of the well-aligned Rydberg orbitals in the nth level as

$$\sigma(n) = \sigma(3)\frac{n}{3}\frac{P(n)}{P(3)}\frac{R_C^2(n)}{R_C^2(3)} = \sigma(3)\frac{n}{3}\frac{P(n)}{P(3)}\frac{(-E(3) - BE_{donor})^2}{(-E(n) - BE_{donor})^2} \quad (17)$$

where we used eq 10 to rewrite the R_C values, and we included the $n/3$ factor to account for contributions from all L-values within a given n. In Table 4, we display the n$P(n)$/(3P(3)) and $R^2_C(n)/R^2_C(3)$ contributions to the cross-section ratios in purple and red, respectively, but only for those electron-transfer events that obey both the surface-crossing and large-penetration conditions. The blank entries in Table 4 belong to events that do not obey these conditions. As in the other tables, bold font is used to label events that clearly meet these criteria; italic font is used to label events that are close to meeting the criteria.

The predictions embodied in Tables 3 and 4 place very strong constraints on which Rydberg levels are expected to be populated in ETD. Only $n = 3-4$ is expected when anion donors having substantial (i.e., greater than a few tenths of an eV) binding energies are used, and even for donors having smaller binding energies, only n between 3 and 7 or 8 is expected. The cross sections for populating $n > 3$ are expected to be larger than for populating $n = 3$ by factors ranging from 15 to greater than 1000.

4. Summary and Overview of Predictions of Our Model

First, it is important to emphasize that the predictions generated from the model described here are not expected to be quantitatively accurate. After all, they are based on crude approximations to the Rydberg and valence (SS σ^* or OCN π^*) orbitals' functional forms, they make the Landau−Zener approximation to the surface-hopping probability, and they ignore effects such as Franck−Condon factors that could act to decrease the hopping probabilities and cross sections. As such, the predictions of our model are best viewed in terms of the *trends* they suggest and the constraints they place on the range of accessible Rydberg levels, and it is these features that we now review.

Probably the most important feature of our model is its insistence that the distance between the anion donor's orbital and the positive site into whose Rydberg orbital the electron transfers obey two conditions *simultaneously*:

1. The distance must obey the *surface-crossing condition* given in eq 10. This condition can be viewed as giving, for a given anion donor with electron binding strength BE_{donor} and for a series of Rydberg energies $E(n)$ appropriate to the positive site, a series of distance $R_C(n)$ that *might* produce electron transfer, but only if the second condition is also met.

2. The second condition is that the surface-crossing distance $R_C(n)$ must lie between $<r> - T/2$ and $<r> + T/2$ for the same Rydberg level that produced this $R_C(n)$. This is what we termed the *large-penetration condition*.

In this paper, we showed that the combination of the above two conditions places severe restrictions on which Rydberg levels will be ETD-populated once one specifies the anion donor's BE_{donor}. Clearly, energy conservation allows only levels obeying $-E(n) > BE_{donor}$ to be populated. However, in addition, as illustrated in Table 2 for values of $-E(n)$ ranging from 4 to 0.1 eV and values of BE_{donor} between 2.5 and 0 eV, the surface-crossing and large-penetration conditions combine to significantly reduce the number of Rydberg levels that can be populated. The results in Table 2 predict that levels with $n > 7$ cannot be populated except by using donors having $BE_{donor} < 0.1$ eV and that, for donors with $BE_{donor} \geq 0.5$ eV, only levels with $n \leq 4$ can be populated. Keeping in mind the qualitative nature of the model we created, we do not claim these limits on n to be quantitatively accurate (i.e., the values of n at which these cutoffs occur may be one or two integers larger). However, we do think the physical content of our model is sufficiently correct to place value in its predicted trends with n and to accept its claim that only rather low n-values can be populated in ETD.

Another important prediction of this model is that the total probabilities $P(n)$ for populating all Rydberg orbitals having quantum number n vary by a factor of only ca. 15 as n ranges from 1 to 8 (see Table 3). As a result, the cross section for electron transfer into all orbitals in the nth Rydberg level, which is given as the probability $P(n)$ for accessing this level multiplied by the surface-crossing cross section πR_C^2, is somewhat more determined by the πR_C^2 factor (see Table 4) than by its $P(n)$ factor. For Rydberg levels with $4 \leq n \leq 5$, the predicted cross sections range from 3 to 140 times the cross section for $n = 3$, which was independently calculated using ab initio methods to be between 3×10^{-2} and 3×10^{-1} Å^2. For $6 \leq n \leq 8$, the cross sections range from 400 to 2200 times that for $n = 3$, but only by using anion donors with very low BE_{donor} can such levels be populated at all.

Combining the new predictions made here relative to anion donor-to-Rydberg electron transfer with the predictions made in refs 38 and 39 using the same model to study Rydberg-to-valence orbital intramolecular electron transfer, we suggest the following mechanism for ETD fragmentation:

1. After forming an orbiting anion−cation complex, the trajectory's eccentricity causes the two oppositely charged ions to periodically come into closer contact. In any such close encounter, initial electron attachment most likely (90−99%) takes place into a Rydberg orbital located on one of the peptide's positive sites, although in a small (1−10%) fraction of the attachment events, the electron can attach directly into SS σ^* or amide π^* orbital. However, such direct orbital attachment can take place only when the orbital is close enough to positive

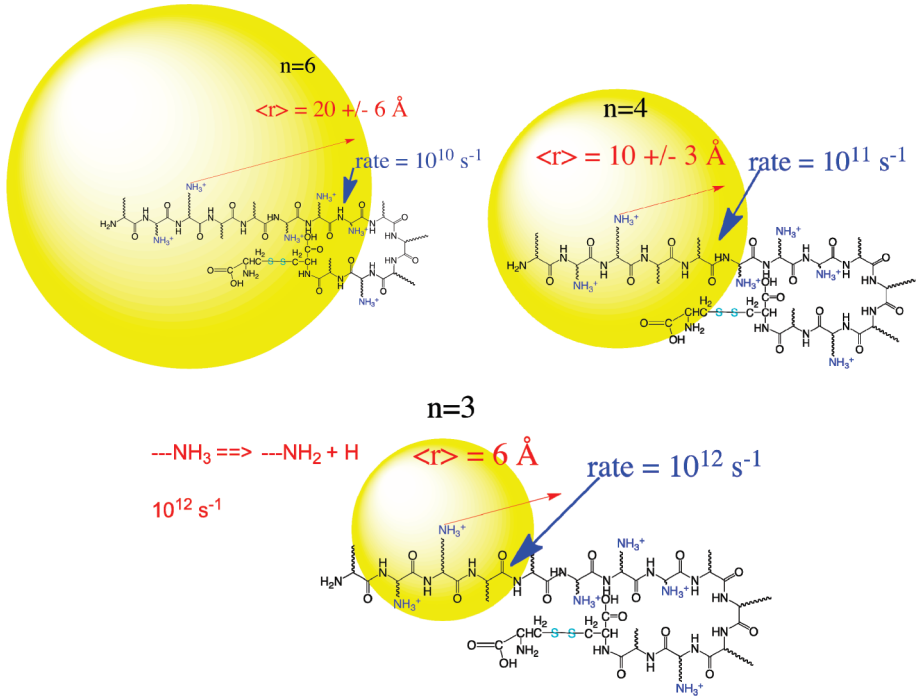

Figure 6. Qualitative depictions of Rydberg orbitals that undergo intramolecular electron transfer (at rates and distances indicated) and to labeled amide π^* sites.

sites to experience sufficient (ca. 1 eV for SS and 2.5 eV for amide) Coulomb stabilization.

2. The Rydberg levels that can be populated using an anion donor of a given electron binding strength BE_{donor} are constrained not only by energy conservation ($-E(n) > BE_{donor}$) but also by the condition that they simultaneously meet the surface-crossing and large-penetration conditions. The combination of these conditions limits ETD to populating only $n < 8$ and only when donors of small BE_{donor} are used; for $BE_{donor} > 0.5$ eV, only levels $n < 4-5$ are expected to be populated.

3. Attachment to any excited Rydberg orbital with $n < 8$, as allowed by the criteria noted above, can be followed by electron transfer from that excited Rydberg orbital to an SS σ^* or amide π^* orbital at rates much in excess of the inter-Rydberg relaxation rate of ca. 10^6 s^{-1}. However, only SS σ^* or amide π^* orbitals that experience differential (relative to the Rydberg site from which the electron is transferred) Coulomb stabilization exceeding 1 or 2.5 eV, respectively, can act as electron acceptors.

4. If a protonated site's ground 3s Rydberg orbital is populated in ETD, prompt (ca. 10^{-10} s or less) H-atom loss ($R\text{-}NH_3 \rightarrow RNH_2 + H$) or NH_3 loss can occur, which thus terminates the possibility of electron transfer from this site to an SS or $N-C_\alpha$ site. In addition, this 3s orbital can transfer its electron to any Coulomb-stabilized SS σ^* or amide π^* orbital within 4.5−6 Å.

5. The only Rydberg orbitals that can transfer electrons to a given SS or amide bond are those that have radial extent $\langle r \rangle \pm T/2$ close to their distance to the SS or amide bond site so that Rydberg-valence orbital overlap penetration is large (if n is too small, the Rydberg orbital does not extend far enough; if n is too large, the valence orbital is too close and thus does not overlap the maximum radial shell of the Rydberg orbital). In addition, the vertical (i.e., near the equilibrium geometry of the parent ion) electron binding energy of the Rydberg orbital must be very similar to the vertical binding energy of the SS σ^*- or amide π^*-attached state (so that the Rydberg-valence state curve crossing occurs near the parent's equilibrium geometry). In Figure 6 we illustrate three Rydberg orbitals having $n < 8$ for which the intramolecular electron transfer rates (given in blue) exceed the relaxation rate. We also show (with blue arrows) those amide sites that lie within the Rydberg orbital's maximum radial shell $\langle r \rangle - T/2 < r < \langle r \rangle + T/2$ and thus are susceptible to accepting an electron.

Note that amide sites that are either too far or too near the center of the Rydberg orbital will not be good electron acceptors for that Rydberg orbital. Finally, for the $n = 3$ case, we remind the reader that N−H or C−N bond cleavage at the protonated amine site occurs (for the 3s state only) at rates comparable to the electron-transfer rate, so these bond cleavages can be expected if the 3s state is populated in the initial ETD event.

6. Although not discussed in this paper, our earlier work suggested that it is also possible for an electron initially attached into an excited Rydberg orbital on one positive site to undergo transfer[26−29] to another Rydberg orbital (having similar or higher electron binding energy) on another positive site. However, transfer to an orbital with a lower electron binding energy cannot occur. Such processes allow attached electrons to migrate throughout the polypeptide. The rates of such Rydberg-to-Rydberg transfers are expected to be largest when the principal quantum numbers of the two Rydberg orbitals are the same and to decrease slowly as the principal quantum numbers of the Rydberg orbitals grow. The Rydberg orbitals most effective in causing the transfer have quantum numbers determined by $R = 2\langle r \rangle_m - T_m$, where R is the distance between the two sites and $\langle r \rangle_m$ and T_m are the radial size and thickness of the optimal Rydberg orbital.

Before closing this section, it is worth reflecting a bit on the similarities and differences between ETD and ECD, even though the latter was not a focus of the present paper. ECD might be expected to populate low-n as well as very high Rydberg levels because one could view a free electron as an anion donor with zero binding energy. In contrast, the surface-crossing and large-

penetration constraints appear to limit ETD to Rydberg levels having $n \leq 7$ or 8. However, ECD and ETD fragmentation patterns and yields are found to be quite similar. So, how can the different range of n-values expected in ETD and ECD still produce similar fragmentation patterns? Although I do not claim to know the answer, it may be useful to offer a few suggestions. One possibility is that ECD can capture into $3 \leq n \leq 8$ Rydberg levels as can ETD, and ECD can also populate higher states, but any Rydberg states having $n >$ ca. 10 formed in ECD relax to lower Rydberg levels (e.g., $n \leq 8$) after which the behavior is as in ETD. It is also possible that instrumental electric fields cause any higher-n Rydberg states formed in ECD to undergo detachment. Another possibility is that the predictions made here for donors with zero electron binding energy can be applied to ECD[43] and thus also place strong limits (from the surface-crossing and large-penetration conditions) on which Rydberg levels ECD can actually access. The author is hesitant to accept the latter speculation because the large-penetration condition that plays a key role in the model offered here to interpret ETD does not appear applicable to ECD. The free electrons used in ECD do not exist in localized valence-size orbitals as they do in ETD. Thermal ($T = 300$ K) free electrons exist in continuum orbitals having de Broglie wavelengths of ca. 70 Å. So, the expression for the penetration integral S given in eq 6 would appear to not apply to ECD; it seems one would need to derive a different expression for the capture cross sections in ECD. So, to this author it still remains a mystery (although the relaxation postulate noted above may explain things) why ECD and ETD yield such similar fragmentations.

In our opinion, the new physical model introduced here and in refs 38 and 39 may offer scientists interested in the atomic-scale mechanisms of ETD (and ECD) an important tool for making predictions as well as a framework for interpreting and understanding fragmentation-pattern data. In this paper, we have put forth several predictions, albeit their quantitative accuracy may be questioned, that beg for experimental testing. For example,

1. It would be helpful to come up with a series of anion donors having similar structural characteristics (so their Franck−Condon factors do not differ much) but a range of BE_{donor} values (e.g., between 0.1 and 0.5 eV).

2. For a small closed-shell cation such as $H_3C\text{-}NH_3^+$, it would be nice to probe the distributions of Rydberg states formed in the initial electron transfer event using several anion donors having BE_{donor} values between 0.1 and 1 eV. Given that the Rydberg levels are expected to have relaxation lifetimes in the μs range and that intramolecular electron transfer cannot occur, these states' populations should be amenable to spectroscopic study.

3. The most obvious experiments would involve using structurally rigid model compounds containing (i) a positively charged site onto which ETD electron transfer can occur and (ii) either a Coulomb-stabilized SS or OCN site or a tag site (e.g., a functional group of significant electron affinity such as used in recent Beauchamp-group experiments[44]) located at a fixed distance (R) from the positively charged group. By varying the BE_{donor} value of the anion donor, one could populate various Rydberg orbitals. Then, by varying R, one could test the large-penetration hypothesis used to derive the results reported here (e.g., SS, OCN, or tag orbitals that are either too far or too close should not accept the Rydberg electron).

Acknowledgment. This work has been supported by NSF Grant No. 0806160.

JA100240F

(43) Because free electrons are intrinsically quantum objects, it is not at all clear that both the Landau−Zener curve crossing condition and the large-penetration condition can be applied, so it is pure speculation that ECD can be viewed as similar to ETD with $BE_{donor} = 0$.

(44) Sohn, C. H.; Chung, C. K.; Yin, S.; Ramachandran, P.; Loo, J. A.; Beauchamp, J. L. *J. Am. Chem. Soc.* **2009**, *131* (15), 5444–5459.